Research Article | Vol. 25, No. 11 | 29 May 2017 | OPTICS EXPRESS 12182

Optics EXPRESS

Demonstration of multiplexed sensor system combining low coherence interferometry and microwave photonics

JESÚS BENÍTEZ, MARIO BOLEA, AND JOSÉ MORA*

ITEAM Research Institute, Camino de Vera, s/n, Edificio 8G, acceso D - Universitat Politécnica de València, 46022, Valencia, Spain
jmalmer@iteam.upv.es

Abstract: In this work, a multiplexed sensor system is proposed by means of the combination of low coherence interferometry (LCI) and microwave photonics (MWP). Variations of physical magnitudes can be measured in an array of head sensors by monitoring the optical path difference generated by each sensor. In this case, the characterization of the multiplexed sensor system is done through the electrical transfer function corresponding to the MWP-LCI system. Moreover, the effect produced by the mutual interaction among head sensors is analyzed in this work. Experimental and theoretical demonstration of the system is provided comparing single detection and balanced detection approaches.

OCIS codes: (280.0280) Remote sensing and sensors; (120.3180) Interferometry; (060.2370) Fiber optics sensors.

References and links

1. C. Y. Chen, C. Y. Wang, and Y. J. Chen, "Analysis of SOI micro ring resonator with reflection property using low coherence interferometry method," in *Proceedings of OptoElectronics and Communication Conference and Australian Conference on Optical Fiber Technology*, pp. 260–262, (2014).
2. H. Liang, B. Peric, M. Hughes, A. Podoleanu, M. Spring, and D. Saunders, "Optical coherence tomography for art conservation and archaeology," Proc. SPIE **6618**, 661805 (2007).
3. W. Drexler, U. Morgner, R. K. Ghanta, F. X. Kärtner, J. S. Schuman, and J. G. Fujimoto, "Ultrahigh-resolution ophthalmic optical coherence tomography," Nat. Med. **7**(4), 502–507 (2001).
4. J. Pluciński, R. Hypszer, P. Wierzba, M. Strąkowski, M. Jędrzejewska-Szczerska, M. Maciejewski, and B. B. Kosmowski, "Optical low-coherence interferometry for selected technical applications," Bull. Pol. Acad. Sci. Tech. Sci. **56**(2), 155–172 (2008).
5. B. Lee, "Review of the present status of optical fiber sensors," Opt. Fiber Technol. **9**(2), 57–79 (2003).
6. A. F. Fercher, W. Drexler, C. K. Hitzenberger, and T. Lasser, "Optical coherence tomography - principles and applications," Rep. Prog. Phys. **66**(2), 239–303 (2003).
7. Y. Wang, J. Gong, D. Y. Wang, B. Dong, W. Bi, and A. Wang, "A quasi-distributed sensing network with time-division multiplexed fiber Bragg gratings," IEEE Photonics Technol. Lett. **23**(2), 70–72 (2011).
8. J. A. Garcia-Souto and H. Lamela-Rivera, "High resolution (<1nm) interferometric fiber-optic sensor of vibrations in high-power transformers," Opt. Express **14**(21), 9679–9686 (2006).
9. N. H. Wan, F. Meng, T. Schröder, R. J. Shiue, E. H. Chen, and D. Englund, "High-resolution optical spectroscopy using multimode interference in a compact tapered fibre," Nat. Commun. **6**, 7762 (2015).
10. J. Capmany and D. Novak, "Microwave Photonics combines two worlds," Nat. Photonics **1**(6), 319–330 (2007).
11. J. Mora, M. Bolea, and J. Capmany, "Novel approach for Low Coherence Interferometry based on a Microwave Photonic architecture," in *Proceedings of International Conference on Transparent Optical Networks*, Mo. C5.2, 1–4 (2015).
12. H. Chen, S. Zhang, H. Fu, B. Zhou, and N. Chen, "Sensing interrogation technique for fiber-optic interferometer type of sensors based on a single-passband RF filter," Opt. Express **24**(3), 2765–2773 (2016).
13. A. L. Ricchiuti, J. Hervás, D. Barrera, S. Sales, and J. Capmany, "Microwave Photonics Filtering Technique for Interrogating a Very-Weak Fiber Bragg Grating Cascade Sensor," IEEE Photonics J. **6**(6), 1–10 (2014).
14. J. Mora, B. Ortega, A. Díez, J. L. Cruz, M. V. Andrés, J. Capmany, and D. Pastor, "Photonic Microwave Tunable Single-Bandpass Filter Based on a Mach-Zehnder Interferometer," J. Lightwave Technol. **24**(7), 2500–2509 (2006).
15. M. Bolea, J. Mora, and J. Capmany, "A novel MWP proposal for low-coherence interferometry applications," in *Proceedings of Microwave Photonics*, 1–4 (2015).
16. C. R. Fernández-Pousa, J. Mora, H. Maestre, and P. Corral, "Radio-frequency low-coherence interferometry," Opt. Lett. **39**(12), 3634–3637 (2014).
17. J. Benítez, M. Bolea, and J. Mora, "High-performance low coherence interferometry using SSB modulation," IEEE Photonics Technol. Lett. **29**(1), 90–93 (2017).

#287862 https://doi.org/10.1364/OE.25.012182
Journal © 2017 Received 7 Mar 2017; revised 20 Apr 2017; accepted 21 Apr 2017; published 15 May 2017

Optics EXPRESS

1. Introduction

Low coherence interferometry (LCI) constitutes a widespread optical technique for high-resolution axial positioning measurement. For the last decades, LCI has been extended to a huge number of application fields such as: optical components characterization [1], art conservation [2], medical diagnosis [3] and sensing [4]. Specifically, in applications related to sensing, a considerable interest in optical fiber sensors has been demonstrated in order to improve the performance of conventional electronic sensors. Mainly, this has been induced by the advantages that optical fiber sensors are able to offer, such as: small and light construction, higher sensitivity and immunity to electromagnetic fields, among others [5].

In the case of sensing applications, those employing LCI principles are based on the measurement of the echo time delay of backscattered light in a head sensor through the characterization of the interference intensity obtained when the light coming from the head sensor and a reference arm overlap. This property is exploited to measure the optical path difference (OPD) by means of a proper transducer located in each head sensor in order to determine the value of different physical magnitudes such as stress, temperature or pressure, among others. When a low coherence source is used, the interference signal is temporally and spatially localized and offers spatial resolutions close to 10 μm [6].

Numerous techniques to implement optical fiber sensors have been developed in order to satisfy a high number of applications. In this way, the most relevant technologies employed are based on fiber gratings [7] and interferometric structures [8], where LCI sensing is included. Typically, schemes based on interferometric structures use optical domain processing in order to obtain the information of the sensor. However, the interference pattern generated in the optical domain is typically affected by environmental variations, which brings instability to the performance of the sensing system [9]. In order to address this issue, the cost and reliability of the schemes are increased by means of a huge design complexity.

In this way, some contributions have been recently proposed with the application of Microwave Photonics (MWP) to sensors. MWP is a technology whose main objective is to improve the capabilities of radiofrequency (RF) engineering by its combinations with the optical technology [10]. The analysis of sensor systems by employing an RF processing, can hugely improve the system performance thanks to the stability of the interference in the RF domain. Concretely, MWP-filtering techniques used initially for optical communication applications [11] have also been addressed for temperature interrogators [12] and strain sensors [13].

In our case, we propose a combination of a LCI sensor-based system and MWP. Several advantages such as better stability of the interference pattern, capability to introduce easily multiplexing techniques or application of post-processing techniques make MWP-LCI a promising solution for this research area. In this work, we propose a novel multiplexed scheme for remote sensor interrogation by means of MWP-LCI technology. The system is based on the RF modulation of a sliced broadband source and the corresponding optical processing through a dispersive element. The structure can measure physical magnitudes such as temperature or stress by monitoring the OPD present in the array of head sensors. In this case, accuracy close to 10 μm can be achieved for each sensor, with a 6 dB amplitude improvement from balanced detection over single detection approaches.

2. Principle of operation

The layout of the proposed MWP-LCI multiplexing sensor structure is shown in Fig. 1. Firstly, a broadband source (BBS) and an optical channel controller (OCC) permit to control the power spectrum distribution of the input optical signal to the system. Afterwards, this signal is double-side band modulated by an RF frequency tone (Ω) provided by a vector network analyzer (VNA). The optical modulated signal is launched into a dispersive element, characterized by its dispersion parameter $\ddot{\varphi}_2$. Following, an interferometric structure is placed

Optics EXPRESS

with the concatenation of two optical couplers. In one of the arms, an array of head sensors is located by means of a 1xN and Nx1 couplers. Each of the 'N' lines that constitute the array of head sensors is composed by an optical circulator to measure the OPD_n produced by each transducer. Additionally, a variable delay line (VDL) is introduced in each line of the array in order to define a working range for each sensor controlled by d_{VDLn}. Since the delay between each sensor is compensated, this parameter allows to directly control the difference in optical delay between adjacent sensors. The performance of the working ranges will be detailed in the following sections. Therefore, this interferometric structure generates the slicing pattern of the optical signal, which is related to the optical path difference OPD_n of each sensor. A control of the optical polarization is considered in the system in order to ensure the maximum visibility of the interference pattern. Finally, a balanced photodetection (BPD) is performed composed of two RF photodiodes, PD1 and PD2. The difference of the RF signals obtained between both photodiodes PD1 and PD2 produces the output RF signal that permits the obtention of the electrical transfer function by means of the VNA. Note that phase information is not needed in our system. Therefore, the experimental requirements could be considerably reduced by introducing a tunable oscillator and an RF detector as replacement for the VNA.

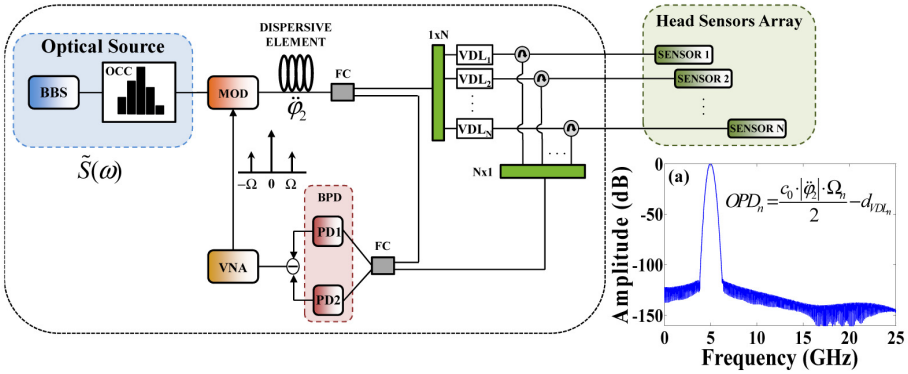

Fig. 1. MWP-LCI multiplexing sensing structure layout. Inset (a) represents an example of the electrical transfer function captured by a VNA when just one sensor is considered and the OPD measured (2.1 mm) produces a RF resonance located at 5 GHz.

Following a similar analysis to the MWP-filtering technique [14], and taking into account the strategic allocation of the interferometer (MZI) before the modulation process [15], the electrical transfer function for single photodetection (SPD) approach is given by:

$$I_{SPD}(\Omega) \approx \underbrace{\sum_n \sum_m H_n H_m^* \cdot \tilde{S}(\Omega - (\Omega_n - \Omega_m)) \cdot e^{-2j\Omega(\tau_n + \tau_m)}}_{DC} \pm \frac{1}{2} I_{BPD}(\Omega) \qquad (1)$$

In the DC term, H_n and H_m represent the amplitude of the magnitude measured at the 'n-th' and 'm-th' sensor, τ_n and τ_m are the optical delays produced inside the corresponding sensor, defined as $\tau_n = OPD_n/c_0 + d_{VDLn}$, and $S(\Omega)$ is the Fourier Transform of the optical source defined as:

$$\tilde{S}(\Omega) = \frac{1}{2\pi} \int_{-\infty}^{\infty} S(\omega) \cdot e^{-j\omega\ddot{\varphi}_2\Omega} d\omega \qquad (2)$$

As can be seen in Eq. (1), a DC term and a contribution corresponding to $I_{BPD}(\Omega)$ are present. The ± sign determines the output of the interferometer, i.e., upper or lower. When a balanced photodetection is performed, the DC term is removed, giving us the expression for the proposed MWP-LCI scheme corresponding to $I_{BPD}(\Omega)$:

Optics EXPRESS

$$I_{BPD}(\Omega) \approx \sum_n H_n \cdot e^{-j\frac{\Omega\tau_n}{2}} \cos\left(\frac{1}{2}\ddot{\varphi}_2\Omega(\Omega-\Omega_n)\right)\cdot\tilde{S}(\Omega-\Omega_n) \quad (3)$$

As shown in Eq. (3), each 'n-th' sensor will produce a RF resonance around the RF frequency Ω_n. Note that the DC term is also removed from the electrical transfer function for an arbitrary number of sensors 'n'. Therefore, any potential residual term produced by interaction of the head sensors is eliminated by using differential detection. The central frequency of this resonance is proportional to the OPD_n measured in each one of the sensors, attending to the following relationship:

$$\Omega_n = \frac{2\left(OPD_n + d_{VDL_n}\right)}{c_0 \cdot \left|\ddot{\varphi}_2\right|} \quad (4)$$

where c_0 represents the speed of light in vacuum and Ω_n is the central frequency of the RF resonance produced by 'n-th' sensor.

In order to show the system performance, Fig. 1(a) plots the theoretical results when one sensor is implemented. As an example, a gaussian profile with 8.8 nm of bandwidth with an accumulated dispersion of $\ddot{\varphi}_2$ = –440 ps^2 is considered. Moreover, the parameter d_{VDLn} has been set to 0 mm. As shown in Fig. 1(a), the electrical transfer function shows an RF resonance close to 5 GHz for an OPD value of 2.1 mm as predicted by Eq. (4). In this way, our proposal permits to obtain the value of different OPDs corresponding to each sensor by monitoring the electrical transfer function of the system. The multiplexing capacity is demonstrated in the following section.

3. Experimental results

Taking into account the MWP-LCI multiplexed structure proposed in Fig. 1, some experimental considerations are done to analyze the system potentiality. The BBS has a total bandwidth of 80 nm. The OCC is centered at 1546.92 nm which is controlled by means of 48 channels with a 0.8 nm bandwidth. The attenuation per channel can be independently modified. In this way, both components BBS and OCC are set to generate a specific power spectrum distribution, S(ω) [15]. Initially, a gaussian profile with 8.8 nm bandwidth is considered. As dispersive element, a standard single mode fiber (SSMF) link is used with an accumulated dispersion of $\ddot{\varphi}_2$ = –440 ps^2. Moreover, the sensor array is particularized by considering two head sensors. For simplicity, the proposed structure is implemented by employing VDLs as head sensors without loss of generality. These VDLs permit to emulate the OPD variations coming from specific transducers for the measurement of real magnitudes such as pressure, temperature and humidity [12]. As abovementioned, the introduction of the parameter d_{VDLn} in each line of the sensor array helps to define several RF operation ranges for each sensor. In this particular case, we set d_{VDL1} = 0 mm and d_{VDL2} = 5 mm. Taking into account the dispersion parameter ($\ddot{\varphi}_2$) from Eq. (4), the operation range for each sensor is determined from 0 to 5 mm. However, the electrical transfer function is limited in a different way from each sensor. In particular, sensor 1 is spectrally defined in the RF domain from baseband to 12.5 GHz whereas sensor 2 is determined from 12.5 to 25 GHz.

Figure 2(a) shows the electrical transfer function of the system when single photodetection is performed. In this case, the values of OPD are adjusted to 4 and 1.1 mm for the sensor 1 and sensor 2, respectively. In Fig. 2(a), we observe different components in the electrical transfer function corresponding to the single detection approach. Firstly, a baseband component (DC term) is present as found in conventional system with single detection [16,17]. It is theoretically described in Eq. (1). Moreover, three additional RF resonances are obtained. Taking into account the relationship between the OPD and the central frequency of each RF resonance, the Eq. (4) predicts that the RF resonances located at f_1 = 10 GHz and f_2 =

Optics EXPRESS

15 GHz correspond to the measurement made by sensor 1 and sensor 2, respectively. However, a third resonance is present around f_{nd} = 5 GHz. This extra resonance is a non-desired contribution produced by the multiplexing architecture of the sensor array as predicted by the DC term of Eq. (1). In a sensor-based system, this additional resonance produces an incorrect measurement since it can be performed as a real change of the physical magnitude under consideration.

Furthermore, the relationship between the OPD and the central frequency of the corresponding resonance is depicted in Fig. 2(b). An excellent linear relationship is found between experimental and theoretical results with a slope of 2.47 GHz/mm.

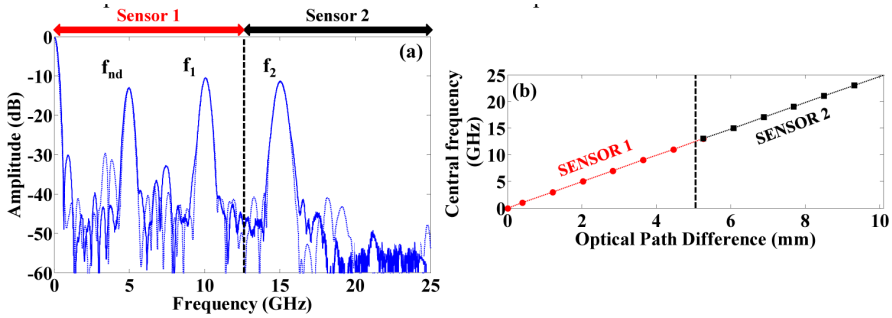

Fig. 2. (a) Electrical transfer function for two multiplexed sensor heads when single detection is considered. Theoretical simulation of Eq. (1) is included in dashed line. (b) Relation between OPD and central frequency of the resonance for each sensor. Theoretical results of Eq. (4) are included in dashed line.

In previous MWP-LCI approaches [16, 17], this non-desired term is not observed since just one sample is considered. Here, we analyze the origin of this residual contribution. A variable attenuator is introduced to control the resonance amplitude of sensor 1. In this way, the resonance amplitude of sensor 2 and the non-desired resonance is measured when the amplitude at sensor 1 is set to different values. The obtained results are shown in Fig. 3(a). As expected, the RF resonance amplitude of sensor 2 is not dependent on sensor 1. Nevertheless, a clear linear relationship between the non-desired resonance amplitude and the amplitude at sensor 1 is observed in Fig. 3(a). Theoretical results are included in dashed lines showing an excellent agreement with the experimental results taking into account the first term of Eq. (1).

Additionally, an experimental analysis of the allocation for the non-desired resonance is provided. Figure 3(b) plots the central frequency of the resonances corresponding to the sensor 1 and the non-desired contribution when different OPDs are set. The OPD at sensor 2 is fixed to 1.1 mm. Comparing both measurements, a linear dependence is found with opposite slopes between the corresponding resonance and the OPD. On the one hand, a linear relationship is observed with a slope of 2.47 GHz/mm related to sensor 1 as predicted by Eq. (4). Therefore, OPD accuracy lower than 10 μm can be achieved with a variation of the central RF frequency close to hundreds of MHz. On the other hand, the allocation of the non-desired term is related to the difference between the frequencies f_1 and f_2 related to both multiplexed sensors. According to Eq. (1), the frequency of the non-desired contribution is $f_{nd} = f_n - f_m$, corresponding to the interaction among sensors n and m through the optical delays τ_n and τ_m, respectively. In this case, an experimental slope of –2.46 GHz/mm is obtained for the non-desired RF resonance. Furthermore, theoretical results are plotted in Fig. 3(b) showing an excellent agreement with the experimental results.

Optics EXPRESS

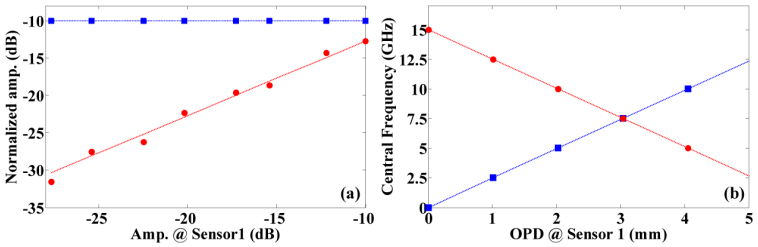

Fig. 3. (a) Amplitude for sensor 2 (■) and non-desired resonance (●) versus the amplitude at sensor 1. (b) Central frequency of the resonance measured at sensor 1 (■) and non-desired resonance (●) versus the corresponding OPD value set at sensor 1. Theoretical simulations are added in dashed line to both figures.

Finally, balanced detection performance is shown in Fig. 4. Comparing with Fig. 2(a), we observe that the baseband component and non-desired contribution are drastically reduced. Therefore, our proposal permits to clearly identify each sensor through a RF resonance without residual contributions. Additionally, an amplitude improvement around 6 dB is achieved in the amplitude measured in each sensor due to the balanced detection. Note that the theoretical simulations are included in dashed line to Fig. 4.

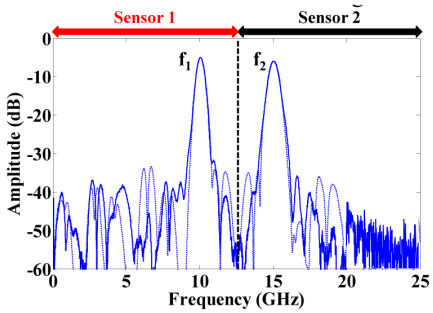

Fig. 4. Electrical transfer function for two multiplexed sensor heads when balanced detection is considered. Theoretical simulation of Eq. (3) is included in dashed line

4. Conclusion

In this work, a multiplexing sensing technique combining MWP and LCI is proposed and experimentally demonstrated. This structure is based on the slicing of a broadband source which is RF modulated and optically processed by means of a dispersive element. The employment of a sensor array in the interferometric structure enables the possibility to obtain measurements of different physical magnitudes by means of the proper transducers. Each sensor, characterized by an OPD value, modifies the electrical transfer function of the MWP-LCI subsystem. An RF resonance can identify each sensor independently when balanced detection is considered. Comparing previous MWP-LCI schemes with single detection, our approach avoids the baseband component and non-desired terms due to the mutual interaction among different sensors. Moreover, an amplitude improvement in the response of each sensor around 6 dB is achieved by performing the balanced detection. Initially, two head sensors are considered in the experimental setup. However, these results can be easily extended to a high number of multiplexed sensors by strategically allocating each head sensor in the RF frequency spectrum.

Funding

National Project TEC2014-60378; Research Excellency Award Program GVA PROMETEO 2013/012.